# SUPPLEMENTAL MATERIAL: EFFECTS OF HYPERVELOCITY IMPACT OF MOLECULES FROM ENCELADUS' PLUME AND TITAN'S UPPER ATMOSPHERE ON NASA'S CASSINI SPECTROMETER FROM REACTIVE DYNAMICS SIMULATIONS

ANDRES JARAMILLO-BOTERO*, QI AN, MU-JENG CHENG, LUTHER W. BEEGLE, ROBERT HODYSS, AND WILLIAM A. GODDARD, III*

## 1. ReaxFF for Ti/C/N/H/O interactions

The ReaxFF force field used in this work was fitted to first principles quantum mechanics (QM) calculations on small motifs to accurately describe compressed states, equilibrium states, and adiabatic dissociative processes. Dissociative states cannot be described with conventional force fields, but they are readily treated with ReaxFF. Thus we fitted ReaxFF to QM calculations of reactants, products, and high-energy intermediates and transition states, using functional forms that behave properly for transition states of chemical reactions and for bond breaking and formation processes. This enables calculations with nearly QM accuracy for large-scale molecular dynamics simulations of chemical reactions under extreme conditions of pressure and temperature, including nonequilibrium energy/mass transfer, decomposition under high strain/heat rates, formation of defects, plastic flow, and phase transitions. In particular the ReaxFF force field is fitted to QM for compressed conditions in order to accurately described the interatomic distances expected from molecular collisions in the velocity regimes reported from Cassini's flybys over the moons of Saturn, Enceladus and Titan.

At high compressions, the potential between two colliding atoms depends on a complex function of interatomic distance, polarization effects, transitions from nuclei-centered to molecular-centered wavefunctions, as well as on the collision velocity (electrons cannot accommodate to the temporal variation of the interaction, e.g. excited or ejected electrons may alter nuclear screening). In contrast full quantum-mechanical calculations have been done only for very few cases, and only in the limit of stationary atoms. The original ReaxFF energy expression formulation, as described in detail in the supplemental material of [2] used a Morse vdW interaction, because the LJ 12-6 has too steep an inner wall and exp-6 has problems at small R. We later found that the Morse serves well to describe the steric effects (nonbond interactions) responsible for determining bond angles and strain in small rings. However for extremely high pressures (regimes >20eV), the inner wall from our conventional ReaxFF energy expression was too soft. Thus the recent generations of ReaxFF [7, 8] include a short-range exponential term of the form $E_{inner} = D\ exp(\alpha(1 - r_{ij}/r_{inner}))$ that is large only for distances much smaller than normal bond energies. The

parameters, $D, \alpha$, and $r_{inner}$, are fitted to QM at short distances. This option is now available in the official LAMMPS distribution, within the Reax/C user package.

To describe bond formation and dissociation, and chemical rearrangements, ReaxFF treats all valence interactions using bond orders derived uniquely from the bond distances, which in turn describe corresponding energies and forces without any discontinuities across reaction pathways. Again all parameters are derived from QM.

In order to describe the changes in bonding during reactions, nonbond interactions are included between all pairs of atoms without two-body and three-body exclusions. Nonbond interactions are of two types, namely electrostatic and van der Waals, which accounts for short range Pauli repulsion and long range dispersion attraction. To avoid energy discontinuities when charged species move in and out of the non-bonded cutoff radius, ReaxFF employs a 7th order distance-dependent Taper polynomial correction starting at $r$=0 and vanishing past $r$=10 Angstroms. The terms in this polynomial are chosen to ensure that all $1^{st}$, $2^{nd}$ and $3^{rd}$ derivatives of the nonbonded interactions to the distance are continuous and go to zero at the cutoff boundary [2].

For our ReaxFF simulations, we assume homolytic ground-state reactions (i.e. no ionization products) and no significant charge separation over large distances away from the impact sites, since we do not expect long-range interactions to play a role under the simulated conditions.

The ReaxFF force field used for this effort, from [**?**] was trained for a number of $TiO_2$ bulk phases including rutile, anatase, brookite, columbite, baddeleyite, fluorite, pyrite, and cotunnite structures, corresponding cold compression equations of state, anatase and rutile water adsorption energy on slab, TiO2 relative energies between phases, anatase and rutile surface energies, anatase water dissociation energies, general oxide heats of formation, finite selected cluster isomers, relative cluster stabilities with respect to most stable form, water addition and rearrangement energies, hydrated cluster growth, rutile water dissociating energies, rutile and anatase cell parameters and charge distribution. This training set was fully verified against the resulting force field and used to re-train for larger inner wall energies versus distances for all interactions. Titanium-carbon, titanium-nitrogen bond-energy bond-distance curves and cold compression equations of state, carbon-titanium-oxygen and nitrogen-titanium-oxygen angle energies, were also added.

An ideal dipole-free $TiO_2$ (rutile) surface was chosen for our simulations because it corresponds to the low-lying energy surface structure for titanium dioxide at room conditions (and lower T and P), hence we expect this phase to be dominant in Cassinis INMS antechamber walls.

A partial set of benchmarked results include bond dissociation curves (Fig. 1), equations of state (Fig. 2), and angles (Fig. 3). Basic mechanical properties for $TiO_2$ bulk (e.g. elastic constants), rutile surface add atom and dissociation energies for carbon, nitrogen, hydrogen and oxygen were also validated against existing experimental data.

The Ti/C/N/H/O ReaxFF force field file used for this work, based on the $TiO_2$-water interactions from [6], is provided as part of the supplemental material files. The implemented version of the ReaxFF engine used for this work has been well validated on numerous materials and applications, including other high-energy phenomena reported in [1, 7, 3, 9, 10].

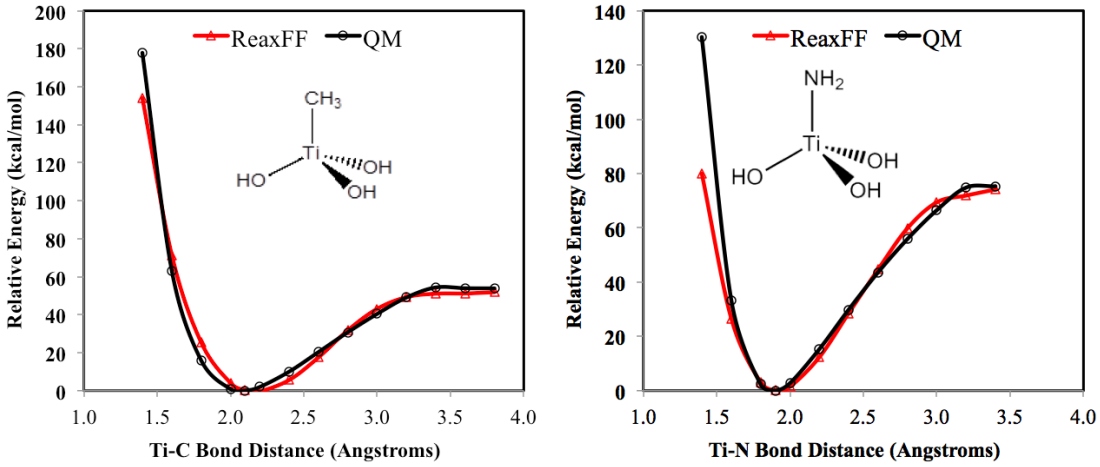


FIGURE 1. Comparison of ReaxFF and QM bond dissociation potential energy surfaces for the Ti-C (left) and Ti-N (right) single bonds in $Ti(OH)_3(CH_3)$ and $Ti(OH)_3(NH_2)$, respectively.

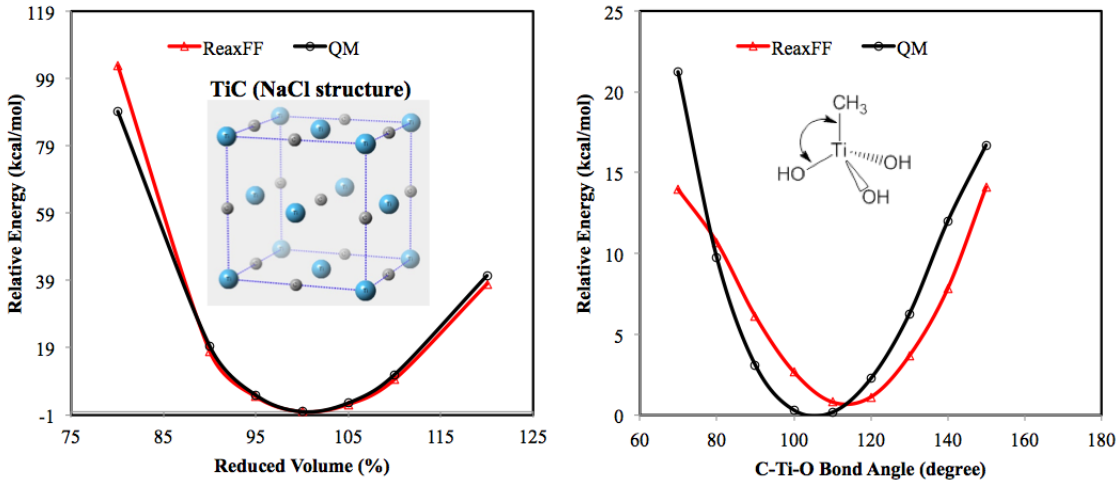


FIGURE 2. (left) Comparison of ReaxFF and QM equation of state (compression/expansion) for the Titanium carbide (TiC), and (right) comparison of ReaxFF and QM valence angle curves for the C-Ti-O angle in $Ti(OH)_3(CH_3)$ molecule.

## 2. Molecular and clathrate fragmentation as a function of impact energy

This section includes tabulated impact simulation data for different molecules and clathrates on a rutile $TiO_2$ surface at the different Enceladus flyby velocities (i.e. E2=8km/s,

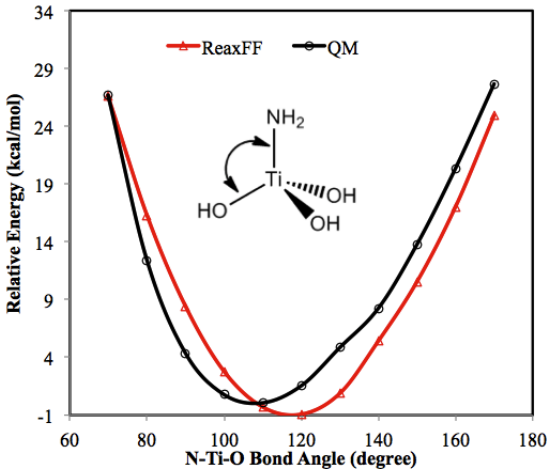


FIGURE 3. Comparison of ReaxFF and QM valence angle curves for the N-Ti-O angle in $Ti(OH)_3(NH_2)$ molecule.

E3=14.41km/s, and E5=17.73km/s), including ice water clusters of different sizes in Table. 1, $CO_2$ ice clathrates in Table. 2, $CO_2$ molecules in Table. 4, methane in Table. 5, and ethylene in Table 6. This data was used to calculate the results reported in the manuscript of this Letter.

TABLE 1. Ice cluster impact (100 times each) on $TiO_2$ surface. H, OH radical are produced in the impact simulations.

| Encounter | cluster radius (Å) | cluster size | $H_2$ | $H_2O$ | $O_2$ |
|---|---|---|---|---|---|
| E2 | 10.5 | 219 | 0 | 193 | 0 |
| E2 | 11.5 | 286 | 0 | 261 | 3 |
| E2 | 12.0 | 334 | 0 | 299 | 3 |
| E2 | 13.0 | 416 | 0 | 367 | 3 |
| E3 | 10.5 | 219 | 17 | 141 | 16 |
| E3 | 11.5 | 286 | 15 | 182 | 19 |
| E3 | 12.0 | 334 | 23 | 214 | 27 |
| E3 | 13.0 | 416 | 33 | 268 | 43 |
| E5 | 10.5 | 219 | 36 | 88 | 44 |
| E5 | 11.5 | 286 | 48 | 118 | 51 |
| E5 | 12.0 | 334 | 60 | 125 | 68 |
| E5 | 13.0 | 416 | 57 | 180 | 75 |

Fig. 4(left) shows the volume mixing fraction between different species produced from clathrates and singular molecules on the $TiO_2$ simulations, and Fig. 4(right) shows the corresponding data from Cassini's INMS from SM in [13]. These results supports the idea

TABLE 2. Clathrate ($CO_2$ + 20 $H_2O$) impact (100 times each) on $TiO_2$ surface. H,OH radicals are produced in the impact simulations. The ratio of $H_2$ over $H_2O$ is much increased compared with pure ice impact which indicate that the impurity in ice plays essential roles in the $H_2$ production. The production of CO is much improved with ice cluster compared with pure $CO_2$ impact indicating that ice cluster can improve the CO production.

| Encounter | $CO_2$ | CO | $H_2$ | $H_2O$ | $O_2$ |
|---|---|---|---|---|---|
| E2 | 40 | 0 | 0 | 1541 | 3 |
| E3 | 40 | 2 | 201 | 921 | 235 |
| E5 | 32 | 7 | 430 | 438 | 558 |

TABLE 3. Comparison of mixing ratios from INMS and ReaxFF simulations at E3 and E5 velocities. The magnitude of $H_2/H_2O$ fraction as a function of velocity agrees with INMS data. The increase in $CO/CO_2$ ratio with velocity is captured for the clathrate but relative magnitude is underpredicted by ReaxFF.

| Molecular species (encounter) | $H_2/H_2O$ | $CO/CO_2$ |
|---|---|---|
| INMS (E3)[13] | 0.22 | 2.75 |
| INMS (E5)[13] | 0.77 | 4.89 |
| ReaxFF $H_2O$[ice] (E3) | 0.11 | - |
| ReaxFF $H_2O$[ice] (E5) | 0.41 | - |
| ReaxFF 20$H_2O$[ice]-$CO_2$ clathrate (E3) | 0.22 | 0.05 |
| ReaxFF 20$H_2O$[ice]-$CO_2$ clathrate (E5) | 0.98 | 0.22 |
| ReaxFF $CO_2$ (E3) | - | 0.00 |
| ReaxFF $CO_2$ (E5) | - | 0.12 |

TABLE 4. $CO_2$ impact (100 times each) on $TiO_2$ surface. O radical is produced in the impact simulations. The number of $CO_2$ is decreasing as impact velocity increase. Only few CO are produced for the highest impact velocity.

| Encounter | $CO_2$ | CO | $O_2$ |
|---|---|---|---|
| E2 | 65 | 0 | 11 |
| E3 | 26 | 0 | 42 |
| E5 | 17 | 2 | 45 |

that the south pole plume at Enceladus contains a high fraction of ice water in the form of clathrates.

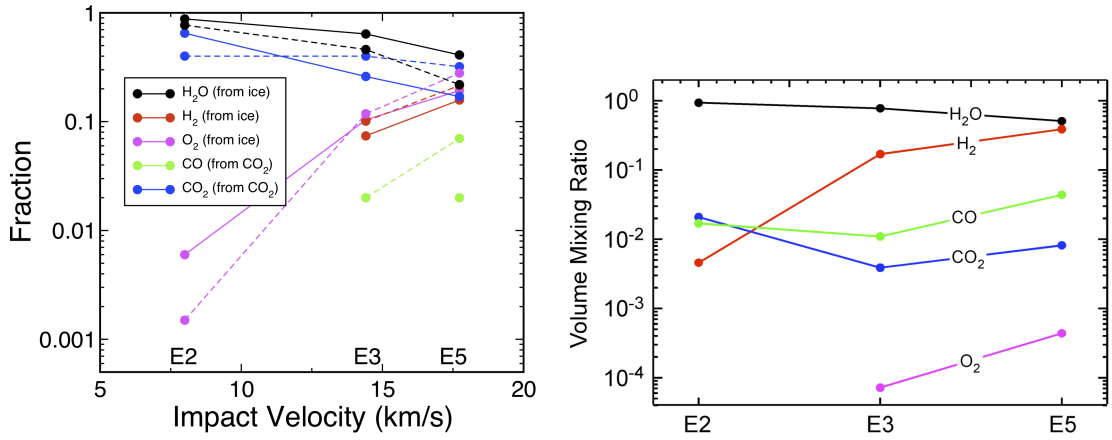


FIGURE 4. (left) Predicted production of fragment species as a function of impactor molecule and impactor velocity. Dotted lines represent ice clathrates with 20 $H_2O$ molecules per corresponding species. $H_2O$ ice impacts lead to an increased production of $H_2$ for E3 and E5 encounters, and of $O_2$ for E2, E3 and E5. CO is produced from $CO_2$ impacts only for E5, while ice water clathrates of $CO_2$ favor CO production even at the lower E3 velocity. In general clathrates increase the fraction of species produced after impact. The total amount of $CO_2$ after $CO_2$ impact decreases for the higher velocity encounters, which suggests part of the observed CO is indeed from the parent $CO_2$. The amount of $CO_2$ from ice clathrates is nearly independent of velocity, while water production decreases with velocity. (right) Mixing ratios as a function of spacecraft speed for the E2, E3, and E5 encounters from Cassini's INMS data.

TABLE 5. $CH_4$ impact (100 times each) on $TiO_2$ surface. H, OH, $CH_3$ radicals are produced in the impact simulations. The main production at high velocity impact are $CH_2O$ and $H_2$.

| Encounter | $CH_4$ | $CH_2O$ | $H_2$ | $H_2O$ | $CO_2$ |
|---|---|---|---|---|---|
| E2 | 61 | 1 | 1 | 0 | 0 |
| E3 | 3 | 12 | 10 | 5 | 0 |
| E5 | 2 | 11 | 9 | 6 | 4 |

## 3. FRAGMENTATION BRANCHING PATHWAYS FOR DIFFERENT IMPACT PROCESSES

Fig. 5 relates fragmentation processes with energy of impact, for encounter velocities between 1-20km/s, calculated from averaged results for the different hexane isomers tabulated in Table 7. The branching pathways are given in % of the corresponding fragmentation

TABLE 6. $C_2H_4$ impact (100 times each) on $TiO_2$ surface. H, OH, $CH_2$ radicals are produced in the impact simulations. CO2 and CO will be produced at high velocity impact.

| Encounter | $C_2H_4$ | $CH_2O$ | $H_2$ | $H_2O$ | $CO_2$ | CO |
|---|---|---|---|---|---|---|
| E2 | 35 | 11 | 1 | 0 | 0 | 0 |
| E3 | 0 | 11 | 10 | 4 | 7 | 1 |
| E5 | 0 | 8 | 12 | 4 | 23 | 5 |

process as a function of impact energy. Velocities are given in km/s and the energies in eV.

Tables 8 (cyclohexane), 9 (hexane), 10 (branched hexane), and 11 (benzene) show additional impact simulations at the Cassini encounter velocities E2,E3, and E5.

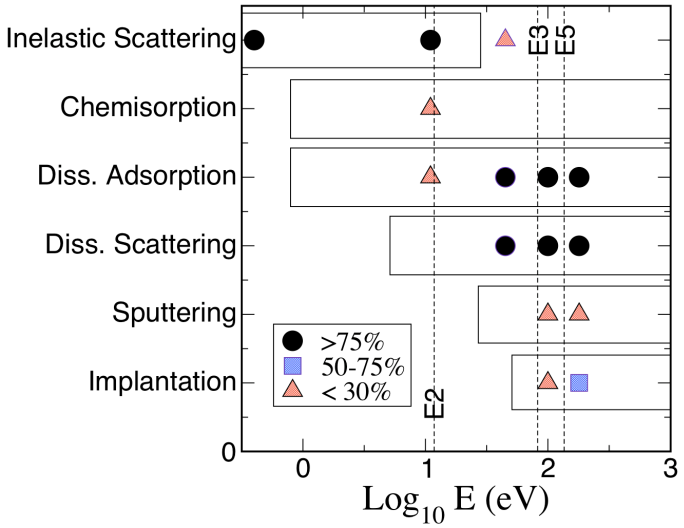


FIGURE 5. Fundamental processes associated with hexane-$TiO_2$ surface collisions. Circles indicate $> 75\%$ branching pathway event probability, the square between 50-75% probability and the triangles $< 30\%$ probability. The rectangular boxes cover the ranges found by [4]. Inelastic scattering has a slight outlier with respect to the data in [4] at 45eV.

## 4. CRATER FORMATION ON RUTILE SURFACE AFTER HV IMPACT OF ICE CLUSTERS

Fig. 6 shows the HV impact effect of ice clusters of various sizes on a $TiO_2$ (110) surface

TABLE 7. The branching pathways counted as number of fragmentation process events for every 100 impacts for hexane isomers as a function of impact energy.

| $E_{\text{col}}$ (in eV) | 0.4 | 11 | 45 | 100 | 180 |
|---|---|---|---|---|---|
| **Hexane** (in km/s) | 1 | 5 | 10 | 15 | 20 |
| Inelastic Scattering | 100 | 91 | 4 | 0 | 0 |
| Chemisorption | 0 | 0 | 0 | 0 | 0 |
| Adsorption (dissoc) | 0 | 9 | 89 | 98 | 100 |
| Dissoc. Scattering | 0 | 5 | 85 | 100 | 100 |
| Sputtering | 0 | 0 | 0 | 4 | 17 |
| Implantation | 0 | 0 | 0 | 20 | 62 |
| **Cyclohexane** | 1 | 5 | 10 | 15 | 20 |
| Inelastic Scattering | 100 | 92 | 3 | 0 | 0 |
| Chemisorption | 0 | 8 | 0 | 0 | 0 |
| Adsorption (dissoc) | 0 | 0 | 87 | 98 | 100 |
| Dissoc. Scattering | 0 | 0 | 79 | 100 | 100 |
| Sputtering | 0 | 0 | 0 | 3 | 26 |
| Implantation | 0 | 0 | 0 | 28 | 66 |
| **Neohexane** | 1 | 5 | 10 | 15 | 20 |
| Inelastic Scattering | 100 | 82 | 7 | 0 | 0 |
| Chemisorption | 0 | 0 | 0 | 0 | 0 |
| Adsorption (dissoc) | 0 | 18 | 87 | 100 | 100 |
| Dissoc. Scattering | 0 | 5 | 77 | 100 | 100 |
| Sputtering | 0 | 0 | 0 | 6 | 19 |
| Implantation | 0 | 0 | 0 | 26 | 72 |

TABLE 8. Cyclohexane ($C_6H_{12}$) impact fragmentation patterns, averaged from 100 different runs, on $TiO_2$ surface. H, OH, $CH_3$ radicals are produced from the impact simulations.

| Encounter | $C_2H_2$ | $CH_2O$ | $H_2$ | $H_2O$ | $CO_2$ | CO | $C_2H_4$ | $C_6H_{12}$ | $O_2$ |
|---|---|---|---|---|---|---|---|---|---|
| E2 | 0 | 14 | 2 | 1 | 0 | 0 | 15 | 6 | 0 |
| E3 | 7 | 51 | 28 | 35 | 23 | 7 | 22 | 0 | 1 |
| E5 | 9 | 27 | 54 | 44 | 38 | 16 | 1 | 0 | 11 |

## 5. eFF ionization during HV impact

From previous work [5], we expect significant electron ionization above the E5 encounter velocities. For this reason we performed additional benchmarking calculations of molecular

TABLE 9. Hexane ($C_6H_{14}$) impact fragmentation patterns, averaged from 100 different runs, on $TiO_2$ surface. H, OH, $CH_3$ radicals are produced in the impact simulations.

| Encounter | $C_2H_2$ | $CH_2O$ | $H_2$ | $H_2O$ | $CO_2$ | CO | $C_2H_4$ | $C_6H_{14}$ | $O_2$ |
|---|---|---|---|---|---|---|---|---|---|
| E2 | 0 | 22 | 0 | 1 | 0 | 0 | 21 | 16 | 0 |
| E3 | 12 | 46 | 54 | 27 | 15 | 9 | 9 | 0 | 2 |
| E5 | 9 | 36 | 73 | 30 | 41 | 15 | 2 | 0 | 17 |

TABLE 10. Branched hexane ($C_6H_{14}$) impact (100 times each) on $TiO_2$ surface. H, OH, $CH_3$ radicals are produced in the impact simulations.

| Encounter | $C_2H_2$ | $CH_2O$ | $H_2$ | $H_2O$ | $CO_2$ | CO | $C_2H_4$ | $C_6H_{14}$ | $O_2$ |
|---|---|---|---|---|---|---|---|---|---|
| E2 | 0 | 14 | 0 | 3 | 0 | 0 | 7 | 14 | 0 |
| E3 | 15 | 54 | 42 | 53 | 10 | 4 | 5 | 0 | 5 |
| E5 | 4 | 29 | 56 | 51 | 38 | 13 | 1 | 0 | 19 |

TABLE 11. Benzene ($C_6H_6$) impact (100 times each) on $TiO_2$ surface. H, OH radicals are produced in the impact simulations. $CH_2O$, $CO_2$, CO are main products at high velocity impact.

| Encounter | $CH_2O$ | $CO_2$ | CO | $H_2$ | $H_2O$ | $O_2$ |
|---|---|---|---|---|---|---|
| E2 | 0 | 0 | 0 | 0 | 1 | 0 |
| E3 | 4 | 19 | 11 | 10 | 9 | 3 |
| E5 | 3 | 54 | 20 | 12 | 8 | 20 |

impacts with a non-adiabatic method capable of describing high energy electronic excitations, the electron force field (eFF). eFF has been validated under extreme conditions of pressure and temperature, well above those possible with ReaxFF, and the results have been the subject of a number of recent publications [11, 12, 5]. Table 12 shows the resulting sub-species after an eFF ethane molecular impact simulation on a hydrogen-capped diamondoid surface.

TABLE 12. Ethane ($C_2H_6$) impact (100 times each) on fixed hydrogen-capped diamondoid using eFF. All fragments including radicals (except H radical) are shown. The impact velocity is 21.22 km/s corresponds to 70 eV, equivalent to the ionization produced by the INMS ionizing gun. This suggest that at these higher impact encounters the amount of ionization produced by the impact is commensurate to that of the ionizer.

| $V_{imp}$ (km/s) | $C_2H_6$ | $H_2$ | $C_2H_4$ | $CH_4$ | $C_2H_5$ | $CH_3$ | CH |
|---|---|---|---|---|---|---|---|
| 21.22 | 18 | 6 | 21 | 1 | 51 | 5 | 4 |

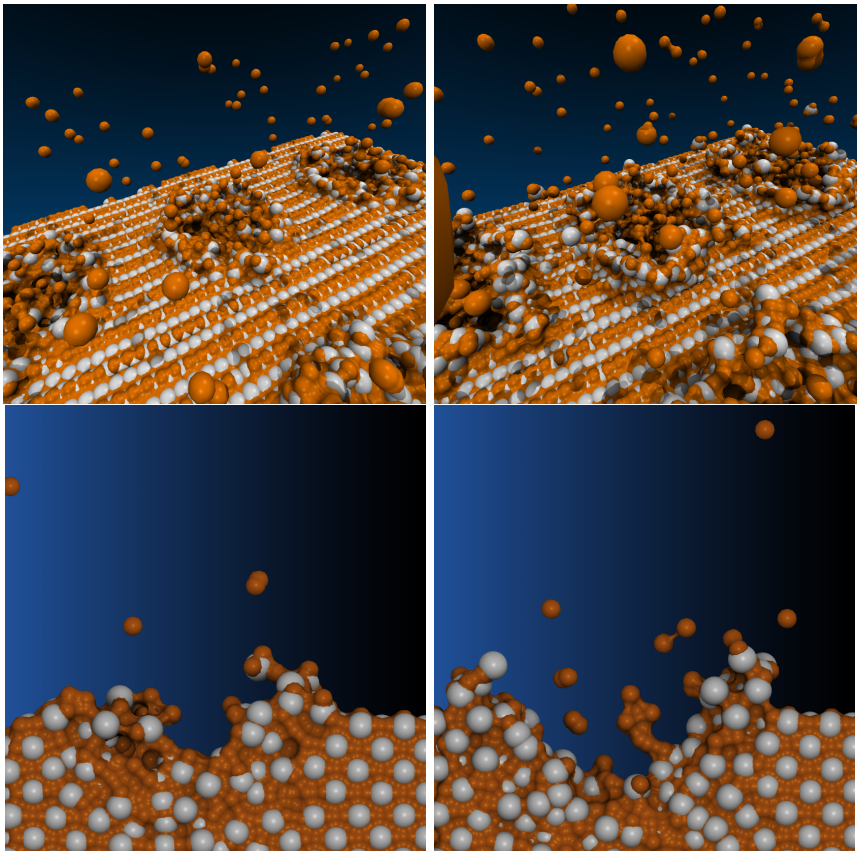

FIGURE 6. Simulated craters caused by HV impact of ice clusters of different sizes on a $TiO_2$ (110) surface. Ti atoms are shown in silver and O in orange, while ice water atoms are removed for clarity. (top-left) 3D crater formed by an ice cluster with 286 waters (i.e. diameter=11.5 Å) at E3 shows surface roughening and Ti surface exposure, (bottom-left) corresponding 2Å slice profile at center of craters, (top-right) crater for same ice cluster at E5, and (bottom-right) corresponding sliced profile. Right figures show a significantly larger crater and Ti emissions for E5.

## 6. Final observations and concluding remarks

We know of no current alternate technologies to ReaxFF (and eFF) for accurately capturing the full range of phenomena that appear under the extreme conditions of hypervelocity impact. That is,

- Current QM is limited both by the length (a few hundred atoms) and time scales (<1ps for QM-MD) of simulation,

- Density functional theory (DFT), the primary QM method used today is also an adiabatic method with very limited capabilities for handling a large number of electronic excitations at finite temperatures (i.e. using curve hoping techniques and TD-DFT variants),
- Conventional force fields, can handle the length and time scales required in these simulations, but cannot handle reaction processes,
- In the extreme of high temperature, Particle In Cell methods are capable of modeling plasma phases with a high fraction of diffuse/ionized electrons,
- At extreme high pressures Path Integral Monte Carlo schemes are capable of statistically sampling thermodynamic states but at a cost that is impractical for studying the dynamics of hypervelocity impact phenomena.

One final observation regarding the use of ReaxFF for highly compressed cases in the velocity regime reported here. We find that the effect of training our ReaxFF force field to higher compression regimes on the chemistry of high energy dissociative reactions is statistically marginal for the range of molecular impacts reported in this Letter, since impact energy is distributed and dissipated among the different degrees of mechanical and chemical freedom, including molecular inelastic scattering and adiabatic fragmentation processes, before non-adiabatic effects become relevant (e.g. electronic ionization). We validated this up to 20eV energies along individual bond directions relative to dissociated states.

## References


1. Q. An, S. V. Zybin, W. A. Goddard, A. Jaramillo-Botero, M. Blanco, and S. N. Luo, *Elucidation of the dynamics for hot-spot initiation at nonuniform interfaces of highly shocked materials*, Physical Review B **84** (2011), no. 22.
2. K. Chenoweth, van Duin A.C.T., Persson P., M. Cheng, Oxgaard J., and Goddard III W.A., *Development and application of a reaxff reactive force field for oxidative dehydrogenation on vanadium oxide catalysts*, Journal of Physical Chemistry C **112** (2008), 14645–14654.
3. S. P. Han, A. C. T. van Duin, W. A. Goddard, and A. Strachan, *Thermal decomposition of condensed-phase nitromethane from molecular dynamics from reaxff reactive dynamics*, Journal of Physical Chemistry B **115** (2011), no. 20, 6534–6540.
4. D. C. Jacobs, *Reactive collisions of hyperthermal energy molecular ions with solid surfaces*, Annual Review of Physical Chemistry **53** (2002), 379–407.
5. A. Jaramillo-Botero, J. Su, A. Qi, and W. A. Goddard, *Large-scale, long-term nonadiabatic electron molecular dynamics for describing material properties and phenomena in extreme environments*, Journal of Computational Chemistry **32** (2011), no. 3, 497–512.
6. S.Y. Kim, P. Persson, N. Kumar, J. Sofo, J.D. Kubicki, and A.C.T van Duin, *Development of a reaxff reactive force field for titanium dioxide/water systems*, Submitted to J. Phys. Chem. A (2011).
7. L. C. Liu, C. Bai, H. Sun, and W. A. Goddard, *Mechanism and kinetics for the initial steps of pyrolysis and combustion of 1,6-dicyclopropane-2,4-hexyne from reaxff reactive dynamics*, Journal of Physical Chemistry A **115** (2011), no. 19, 4941–4950.
8. L. C. Liu, A. Jaramillo-Botero, H. Sun, and W. A. Goddard, *Development of a reaxff reactive force field for ettringite and study of its mechanical failure modes from reactive dynamics simulations*, J Phys. Chem. A (DOI: 10.1021/jp210135j, March 13, 2012).

9. L. C. Liu, Y. Liu, S. V. Zybin, H. Sun, and W. A. Goddard, *Reaxff-/g: Correction of the reaxff reactive force field for london dispersion, with applications to the equations of state for energetic materials*, J. Phys. Chem. A **115** (2011), no. 40, 11016–11022.
10. J. E. Mueller, A. C. T. van Duin, and W. A. Goddard, *Development and validation of reaxff reactive force field for hydrocarbon chemistry catalyzed by nickel*, Journal of Physical Chemistry C **114** (2010), no. 11, 4939–4949.
11. P. L. Theofanis, A. Jaramillo-Botero, W. A. Goddard, T. R. Mattsson, and A. P. Thompson, *Electron dynamics of shocked polyethylene crystal*, Physical Review B **85** (2012), no. 9.
12. P. L. Theofanis, A. Jaramillo-Botero, W. A. Goddard, and H. Xiao, *Nonadiabatic study of dynamic electronic effects during brittle fracture of silicon*, Physical Review Letters **108** (2012), no. 4.
13. J. H. Waite, W. S. Lewis, B. A. Magee, J. I. Lunine, W. B. McKinnon, C. R. Glein, O. Mousis, D. T. Young, T. Brockwell, J. Westlake, M. J. Nguyen, B. D. Teolis, H. B. Niemann, R. L. McNutt, M. Perry, and W. H. Ip, *Liquid water on enceladus from observations of ammonia and (40)ar in the plume (vol 460, pg 487, 2009)*, Nature **460** (2009), no. 7259, 1164–1164.